Chinese Chemical Letters 36 (2025) 109922

Contents lists available at ScienceDirect

Chinese Chemical Letters

journal homepage: www.elsevier.com/locate/cclet

A single-component LED excited enone photoinitiator for colorless and transparent antibacterial film preparation

Lingfeng Zheng, Chengyuan Lv, Wenlin Cai, Qingze Pan, Zuokai Wang, Wenkai Liu, Jiangli Fan*, Xiaojun Peng

State Key Laboratory of Fine Chemicals, Frontier Science Center for Smart Materials, Dalian University of Technology, Dalian 116024, China

ARTICLE INFO

Article history:
Received 8 March 2024
Revised 19 April 2024
Accepted 23 April 2024
Available online 24 April 2024

Keywords:
Single-component photoinitiator
Photobleaching
Low-migration
Cytocompatibility
Photopolymerized antibacterial film

ABSTRACT

Photoinitiators (PIs), as the key substances for photopolymerized antibacterial film (PAF), affect the cure rate and color of PAF. Herein, two enone dyes were designed and synthesized by a facile approach. Among the candidates, BDO1 has demonstrated the ability to initiate polymerization of acrylate monomers as single-component PI with the advantages of low mobility, outstanding photobleaching, excellent cytocompatibility, and suitability for light emitting diode (LED) light sources above 365 nm. Taking BDOs as examples, a novel method based on theoretical calculations aiming to assess the potential of enone molecules as single-component PIs was proposed. Finally, under the initiation of BDO1, tannic acid was photopolymerized to a colorless and transparent antibacterial film with high antibacterial ability, which indicated that BDO1 was expected to be used in environmentally friendly PAF.

Bacterial infections have seriously affected people's health and quality of life [1–3]. In order to deal with various bacterial infections, people have been committing to new and efficient antibacterial materials [4–7]. Antibacterial film is a new type of active material, which can effectively prevent bacterial infections and has been widely used in medicine and food [8,9]. At present, the preparation methods of antibacterial film mainly include solvent evaporation, plastic molding, and physical vapor deposition [10–12]. However, these methods have shortcomings such as high thermal stability requirements for antibacterial agents and long preparation time [13].

Photopolymerized antibacterial film (PAF) has attracted much attention because photopolymerized antibacterial monomers (PAMs) can achieve rapid cross-linking curing initiated by the photoinitiators (PIs) under light irradiation [14,15]. The PIs, as the key component for polymerized reaction, are critical to the cure rate and color of the PAF [16]. Compared with cationic PIs, free radical PIs have the advantages of being inexpensive, diversified, and easier to realize spatial controllability, so free radical PIs are currently the most popular ones [17]. Mercury lamps, as the traditional light source for polymerization, are gradually restricted due to environmental pollution and short service life [18]. Light emitting diode (LED) light sources make up for the above shortcomings [19,20]. However, due to the limitation of LED technology, LED lights with emission wavelength below 365 nm have low light efficiency and short lifespan [21,22]. Compared with type I PIs (lysis free-radical), type II PIs (hydrogen abstraction) show better absorption characteristics at wavelengths above 365 nm and better match common LED light sources [23]. Unfortunately, most type II PIs are cumbersome to synthesize and are often used in combination with co-initiators resulting in complex compositions [24,25]. In addition, migration to the surface *via* the interior of the cured object may be hazardous to human health [26,27]. Two strategies have been proposed to reduce the mobility of PIs [28–35]. One approach involves incorporating unsaturated groups to enable the participation of PIs in the polymerization reaction, while the other method entails increasing the molecular weight of PIs to impede their migration. However, the solubility and initiation efficiency of macromolecular PIs need to be further improved [33,36,37]. Therefore, it is of great significance to develop easily synthesized single-component LED-excited small molecule type II PIs with low mobility.

Enone molecules are simple to synthesize and purify, and have been reported as type II PIs with good initiating effects [38–42]. Although there are some studies on single-component enone PIs, they contain alkylamino groups which could cause yellowing and odor in the cured product [43–47]. Based on the above-mentioned concerns, by introducing the piperone ring without an alkylamino

* Corresponding author.
E-mail address: fanjl@dlut.edu.cn (J. Fan).

https://doi.org/10.1016/j.cclet.2024.109922
1001-8417/

Table 1
Photophysical properties of BDOs.

PI	$\lambda_{max,abs}$[a] (nm)	$\varepsilon_{@max}$[a] (10^4 L mol^{-1} cm^{-1})	$\varepsilon_{@365\,nm}$[a] (10^4 L mol^{-1} cm^{-1})	$\varepsilon_{@385\,nm}$[a] (10^4 L mol^{-1} cm^{-1})	$\varepsilon_{@395\,nm}$[a] (10^4 L mol^{-1} cm^{-1})	$\varepsilon_{@405\,nm}$[a] (10^4 L mol^{-1} cm^{-1})	Φ_f[b]
BDO1	370	3.754	3.706	3.040	2.143	1.233	0.2%
BDO2	368	3.409	3.396	2.682	1.855	1.062	0.4%

[a] Measurements were performed in CH_3CN.
[b] Absolute fluorescence quantum yield in dichloromethane (DCM) (excited by $\lambda_{max,abs}$).

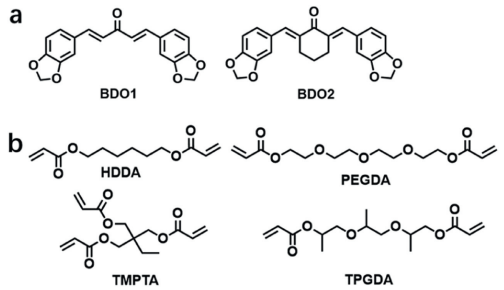

Fig. 1. (a) Structures of BDOs in this work. (b) Structures of commercial monomers.

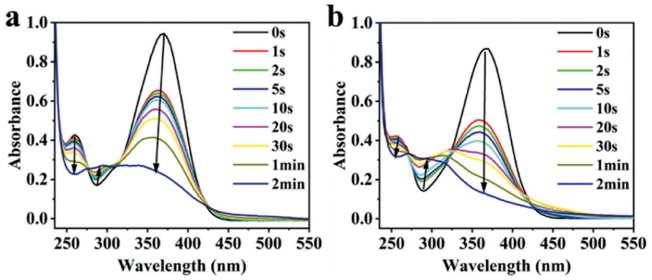

Fig. 2. UV–vis absorption spectra obtained upon the photolysis of (a) BDO1, (b) BDO2, upon irradiation at 365 nm. Light intensity: 100 mW/cm^2.

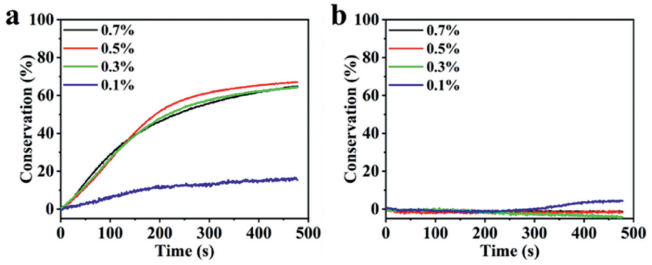

Fig. 3. Conversion of double bond initiated by different content of BDOs in HDDA at LED@365 nm under illumination. (a) BDO1, (b) BDO2, weight fraction relative to monomer, the light intensity was set to 100 mW/cm^2.

group as the hydrogen donor, we synthesized two enone dyes (BDOs). The only difference between the two molecules was that BDO2 introduced a six-member ring on ketone part to discuss the effect of increasing molecular rigidity on the photoinitiation efficiency [48–50]. BDO1 could be used as a single-component PI to initiate the polymerization of acrylate monomers with the advantages of low migration, splendid photobleaching, and remarkable cytocompatibility under commercial LED light sources. Photolysis, electron spin resonance (ESR), and free radical photopolymerization were carried out to estimate their photopolymerization behaviors. In addition, taking BDOs as examples, a novel method based on theoretical calculations was proposed, aiming to assess the potential of enone molecules as single-component PIs. Finally, BDO1 was successfully used to prepare colorless and transparent PAF with an excellent antibacterial effect.

Tannic acid, a natural plant polyphenol, was renowned for its antioxidant, antibacterial, anti-inflammatory, and biodegradable properties [51,52]. Compared to other antibacterial materials, tannic acid possessed the advantage of biodegradability [53]. We modified tannic acid to prepare photosensitive tannic acid as PAM. BDOs and photosensitive tannic acid (PSTA) were prepared *via* a simple synthetic route as shown in Scheme S1 (Supporting information). ^{1}H NMR spectra, ^{13}C NMR spectra, high-resolution mass spectra, and Fourier transform infrared (FT-IR) spectra were shown in Figs. S8–S15 (Supporting information). The molecular structures of BDOs were shown in Fig. 1a. HDDA, PEGDA, TMPTA and TPGDA (Fig. 1b) as commercial monomers were used to verify the ability of BDOs to initiate acrylate monomers.

As illustrated in Fig. S1 (Supporting information), the absorption peaks of BDOs were almost coincident, and exhibited high molar absorption coefficients ($>3\times10^4$ L mol^{-1} cm^{-1}) at 365 nm (Table 1), which meant BDOs could be excited by commercial ultraviolet (UV) LED light sources. Both the fluorescence quantum yields of BDOs were very low (<1%) (Table 1), which was more favorable for free radical generation.

Generally, the rate of photolysis tends to positively correlate with photo-initiation ability [17]. Thus, the photolytic behavior of BDOs upon irradiation with a 365 nm LED was studied (Fig. 2). Notably, a rapid decline of UV–visible (UV–vis) absorption spectroscopy at 365 nm was detected along with a new absorption peak appearance at 285 nm, which indicated that BDOs underwent photolysis and had the potential for photobleaching.

Then the photopolymerization kinetics of HDDA as the monomer and BDOs as the PI were investigated by real-time FT-IR (Fig. 3). The results indicated that BDO1 but not BDO2 could effectively initiate polymerization. As shown in Fig. 3a, an increase in irradiated BDO1 up to 0.3 wt% amplified the free radical production and thus increased the double bond conversion. However, at 0.5 wt%, the rate of polymerization increased slightly, which was attributed to the excessive production of free radicals, thus accelerating the termination of the reaction. Fig. 3b illustrated that the double bond conversion of HDDA initiated by BDO2 was almost 0, indicating that BDO2 could not effectively initiate the polymerization of HDDA.

Finally, the polymerization behavior of 0.3 wt% BDO1 in different monomers was further investigated (Fig. S2 in Supporting information). The final double bond conversions (8 min irradiation) of commercial monomers (TPGDA, HDDA, PEGDA, TMPTA) induced by BDO1 were 73%, 64%, 57%, and 24%, respectively. Interestingly, the double bond conversion rate of difunctional monomers (TPGDA, HDDA, PEGDA) surpassed that of trifunctional monomers (TMPTA). Conversely, the initiation rates, as represented by the slope of the double bond conversion rate curve, demonstrated an inverse relationship. This phenomenon was in line with the general nature of monomers. That is to say, the initiation rate was positively correlated to the functionality, but as the functionality increased, the viscosity increased, which was not conducive to free radical diffusion, resulting in a low double bond conversion rate.

Subsequently, the photochemical reaction of BDO1 was investigated. Following the paradigm of the photochemical reactions of

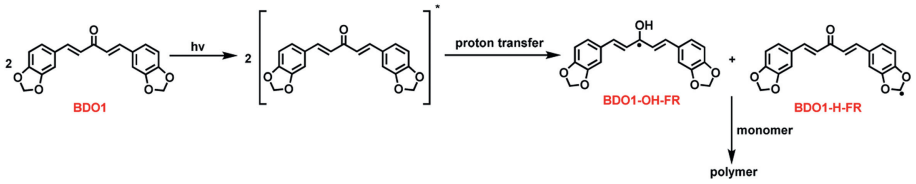

Scheme 1. Proposed mechanisms of the radicals generated through hydrogen transfer from the BDO1.

the carbonyl compounds, σ(C–H) bond from the half full highest occupied molecular orbital (HOMO) attacked the C=O group in the half full lowest unoccupied molecular orbital (LUMO) [54–57]. Past studies suggested the methylene group in the peppercorn ring could act as a hydrogen donor [17]. Therefore, the most plausible photoinitiation process mechanism was proposed (Scheme 1).

ESR and real-time ^{1}H NMR experiments were conducted for further insight into the photochemical reaction mechanism. The solution of BDO1 was irradiated by LED@365 nm for 15 min. A free radical was captured by the *N*–*tert*–butyl–α-phenylnitrone (PBN) in Fig. S3a (Supporting information), with hyperfine coupling constants of $a_N = 14.2$ G and $a_H = 2.2$ G, and it was assigned to the BDO1-H-FR radical (Scheme 1) [58]. Due to the significant steric hindrance exhibited by the BDO1-OH-FR radical, PBN failed to capture it. This observation further suggested that, owing to steric hindrance, BDO1-OH-FR was incapable of initiating monomer polymerization, with BDO1-H-FR assuming the role of initiator instead. Subsequently, BDO1 was dissolved in $CDCl_3$ under N_2 atmosphere, the solution was irradiated with LED@365 nm, and ^{1}H NMR spectra were measured every minute (Fig. S4 in Supporting information). After 4 min of irradiation, the characteristic peaks of the methylene of BDO1 (6.02 ppm) gradually weakened. Meanwhile, the broad peak at 6 ppm gradually increased, which could be attributed to the O–H protons on the hydroxyl group. The change in peak displacement of the aromatic region demonstrated the coupling reaction of the radicals produced by BDO1. ESR and real-time ^{1}H NMR experiments showed that the BDO1 carbonyl group extracted the proton of the methylene group, generating BDO1-H-FR radical and BDO1-OH-FR radical.

Theoretical calculation was also conducted to validate the rationality of the proposed mechanism, and the simplified Jablonski diagram of BDO1 was obtained using density functional theory (DFT) and time-dependent DFT (TD-DFT) calculations (Fig. 4a). BDO1 was excited from a ground state (S_0) to an excited singlet state (S_1) and then relaxed to the $^*S_1$ state by vibrational relaxation (Vr). The $^*S_1$ state underwent intersystem crossing (ISC) to the triplet state (T_3, T_2, and T_1). Table S1 showed the frontier molecular orbital (FMO) of BDO1 in different states. The energy gap between $^*S_1$ and T_3 states was lower and the spin-orbit coupling (SOC) was larger, favoring the ISC of singlet to triplet state. Subsequently, we calculated the reaction energies of BDO1 in different states by computing the difference between the total energy of the products and the total energy of the reactants (Table 2 and Table S3 in Supporting information). In the ground state, BDO1 showed positive reaction

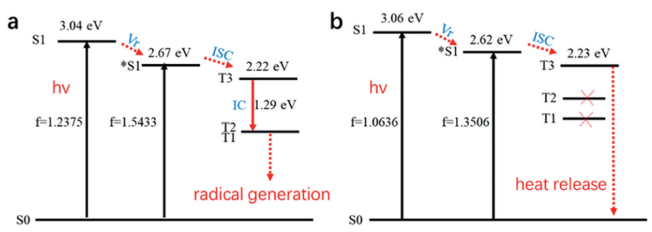

Fig. 4. Simplified Jablonski diagram of BDOs: (a) BDO1, (b) BDO2.

Table 2
Calculated reaction energies of BDO1 in the ground state and excited states (kcal/mol).

PI	S_0	S_1	T_3	T_2	T_1
BDO1	43.12	−91.13	−80.20	−36.40	−36.40

energies, suggesting an improbable occurrence of reactions. Conversely, in the S_1, T_3, T_2, and T_1 states, ΔE values were negative. We hypothesized that BDO1 in the S_1 state preferred ISC without generating free radicals. This supposition was supported by the low absolute fluorescence yield (Table 1) and different ESR spectra under air and nitrogen conditions (Fig. S3 in Supporting information). Therefore, we inferred that the photochemical reactions most likely occurred in the triplet states. The process of generating free radicals was deduced using the FMO theory and the principle of maximum orbital overlap (Fig. S5 in Supporting information). In the T_3 state, hindered FMO interaction between the σ(C-H) bond and the p orbital of the C=O group, along with a larger energy gap between HOMO-2 and LUMO, made the reactions unfavorable. However, in the T_1 state, with a half-full HOMO and LUMO and the smallest energy gap, ideal π-π^* FMO interaction between the σ(C-H) bond and the π orbital of C=O allowed for maximum orbital overlap. Theoretical calculations demonstrated that BDO1 could produce BDO1-H-FR radical and BDO1-OH-FR radical and the photochemical reactions occurred in the T_1 state.

Due to the inherent rigidity of the BDO2 ketone part, the optimization of the T_2 and T_1 states led to structural destruction (Table S2 in Supporting information), resulting in the S_0, S_1 and T_3 states without any reasonable T_2 and T_1 states (Fig. 4b). Similar to BDO1, BDO2 in the S_0, S_1, and T_3 states was unfavorable for free radical generation. Experimental observations revealed that when BDOs were dissolved in chloroform under 365 nm LED lamps for 2 min, the solution of BDO2 began boiling and frothing, demonstrating that a significant thermal effect was generated due to the rapid rotation of the molecular structure. Furthermore, the hyperfine coupling constants of the PBN adducts for BDO2 (Fig. S3c) were determined to be $a_N = 14.2$ G and $a_H = 2.5$ G, distinct from those of BDO1 (Fig. S3a), which could generate free radicals capable of initiating monomer polymerization, further confirming that BDO2 cannot initiate monomer polymerization. Those indicated the unsuitability of BDO2 as a PI. Therefore, by decreasing the rigidity of the ketone in enone molecules, internal conversion rates and the production of free radicals could be increased, thereby enhancing their ability to initiate monomers as single-component PIs.

In light-curing systems, incomplete reaction of PIs could result in the migration of unreacted PIs to the coating surface over time, posing environmental and health risks [30]. Therefore, evaluating the migration stability of BDO1 becomes imperative. To assess this, polymers initiated by BDO1 using various monomers were prepared and subsequently ground into powder. Acetonitrile was used to extract residual BDO1 from the powder, and the migration rate was analyzed through UV–vis absorption spectrum measurements (Fig. S6 and Table S5 in Supporting information). The unsaturated double bond within BDO1 actively participated in polymerization and became integrated within the polymer network, effectively re-

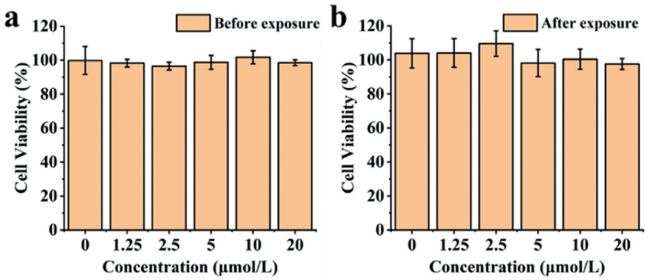

Fig. 5. Cytotoxicity under 24 h of treatment under various concentrations (0–20 μmol/L) of BDO1. (a) Before exposure, (b) after exposure. Cos-7 cells were used in the cytotoxicity experiments. Data are presented as mean ± standard deviation (SD) ($n = 6$).

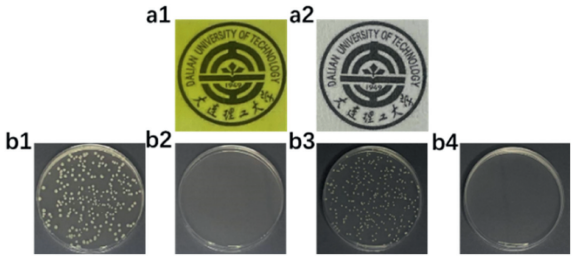

Fig. 6. Antibacterial films composed of BDO1 and PSTA: (a1) before exposure, (a2) after exposure. Photographs of bacteria colonies grown on the solid LB agar plates: (b1, b2) *E. coli*, (b3, b4) *S. aureus*. (b1, b3) Blank control. (b2, b4) Treated with antibacterial film made of BDO1 and PSTA.

ducing the migration of small-molecule to the polymer surface. Consequently, the observed very low mobility (<0.2%) and utilization rate (0.3 wt%) of BDO1 signified its significant potential for application in the field of PAF.

With the expanding use of PAF in food packaging and biomedicine, evaluating the biocompatibility of PIs becomes crucial. We assessed the *in vitro* cytotoxicity of BDO1 on Cos-7 cells using the MTT colorimetric assay. Notably, even with an increase in BDO1 concentration from 1.25 μmol/L to 20 μmol/L, cell viability consistently remained at 98% (Fig. 5a), similar to cell survival rates observed during DMSO treatment. In addition to analyzing the cytotoxicity of the BDO1 itself, we investigated the cytocompatibility of photolysis products irradiated at LED@365 nm (Fig. 5b). Compared with that of BDO1 before irradiation, cellular metabolic activity was not reduced after irradiation under treatment with the same concentration. BDO1 showed low cytotoxicity, demonstrating its favorable biocompatibility.

The photopolymerization kinetics of PSTA initiated by BDO1 was investigated using real-time FT-IR. After 8 min of illumination, the final double-bond conversion could reach 60% (Fig. S7 in Supporting information), indicating that BDO1 could independently serve as a PI to initiate PSTA polymerization. Subsequently, we applied the photosensitive solution consisting of BDO1 and PSTA on a slide (Fig. 6, a1), resulting in a colorless and transparent film post-exposure (Fig. 6, a2).

To evaluate the antibacterial properties of PAF, antibacterial assays of the film against *Escherichia coli* (*E. coli*, Gram-negative bacteria) and *Staphylococcus aureus* (*S. aureus*, Gram-positive bacteria) were conducted. The optical images of bacterial colonies were captured 24 h after their incubation on the solid agar surface. The treated bacterial suspension did not grow colonies (Fig. 6, b2 and b4), while the untreated bacterial suspension grew a large number of bacterial colonies on the agar surface (Fig. 6, b1 and b3). This highlighted the film resulting from the photopolymerization of the photosensitive solution containing BDO1 and PSTA exhibited highly effective antibacterial properties, with an antibacterial rate as high as 99.9%. Therefore, BDO1 demonstrated significant potential for application in PAF.

In conclusion, two enone dyes were synthesized in this work, among which BDO1 could be used as single-component PI to initiate the polymerization of common monomers (HDDA, PEGDA, TMPTA, TPGDA) and the polymers formed are light in color. BDO1 possesses the advantages of simple preparation, low migration, photobleaching, high biocompatibility, and matching with common LED light sources. Furthermore, we established a theoretical approach to demonstrate that rigid structures had a detrimental effect on photoinitiation efficiency. Finally, under the initiation of BDO1, tannic acid was photopolymerized to a colorless and transparent antibacterial film with high antibacterial ability. We anticipate that BDO1 with low migration, outstanding photobleaching, and excellent biocompatibility properties will possess great potential for PAF preparation in the future.

Declaration of competing interest

The authors declare that they have no known competing financial interests or personal relationships that could have appeared to influence the work reported in this paper.

CRediT authorship contribution statement

Lingfeng Zheng: Writing – original draft, Methodology, Investigation, Data curation. **Chengyuan Lv:** Investigation, Data curation. **Wenlin Cai:** Investigation, Data curation. **Qingze Pan:** Investigation, Data curation. **Zuokai Wang:** Investigation, Data curation. **Wenkai Liu:** Investigation. **Jiangli Fan:** Writing – review & editing, Funding acquisition. **Xiaojun Peng:** Investigation.

Acknowledgments

This work was financially supported by National Natural Science Foundation of China (Nos. 21925802, 22338005), Liaoning Binhai Laboratory (No. LBLB-2023–03) and the Fundamental Research Funds for the Central Universities (No. DUT22LAB601).

Supplementary materials

Supplementary material associated with this article can be found, in the online version, at doi:10.1016/j.cclet.2024.109922.

References

[1] W. Liu, H. Gu, W. Liu, et al., Chem. Eng. J. 450 (2022) 137384.
[2] W. Su, X. Luo, P. Li, et al., Chin. Chem. Lett. 35 (2024) 109522.
[3] L. Zhao, X. Guo, Z. Zhang, et al., Chin. Chem. Lett. 35 (2024) 109506.
[4] B. Ran, L. Ran, Z. Wang, et al., Chem. Rev. 123 (2023) 12371–12430.
[5] B. Ran, Z. Wang, W. Cai, et al., J. Am. Chem. Soc. 143 (2021) 17891–17909.
[6] S. Li, Z. Li, Q. Hao, et al., Chin. Chem. Lett. 35 (2024) 108636.
[7] Z. Li, Q. Feng, J. Shen, Chin. Chem. Lett. 35 (2024) 109602.
[8] T. Li, X. Zhang, J. Mei, et al., Front. Microbiol. 13 (2022) 860123.
[9] D. Zhang, S. Cheng, J. Tan, et al., Bioact. Mater. 17 (2022) 394–405.
[10] B. Feng, S. Zhang, D. Wang, et al., Prog. Org. Coat. 165 (2022) 106766.
[11] C. He, Q. Chen, M.A. Yarmolenko, et al., Prog. Org. Coat. 123 (2018) 282–291.
[12] X. Huang, X. Zhou, Q. Dai, et al., Nanomaterials 11 (2021) 3337.
[13] M.O. Mavukkandy, S.A. McBride, D.M. Warsinger, et al., J. Membr. Sci. 610 (2020) 118258.
[14] A. Kraśkiewicz, A. Kowalczyk, K. Kowalczyk, et al., Prog. Org. Coat. 187 (2024) 108141.
[15] S. Kumaran, E. Oh, S. Han, et al., Nano Lett. 21 (2021) 5422–5429.
[16] Y. He, J. Luckett, B. Begines, et al., Biomaterials 281 (2022) 121350.
[17] X. Ren, W. Liu, Q. Yao, et al., Dyes Pigm. 200 (2022) 110133.
[18] Z. Tang, Y. Gao, S. Jiang, et al., Prog. Org. Coat. 170 (2022) 106969.
[19] Q. Pan, S. Wang, X. Ren, et al., Chem. Eng. J. 477 (2023) 147104.
[20] L. Tang, J. Nie, X. Zhu, Polym. Chem. 11 (2020) 2855.
[21] I. Beliakova, V. Piscio, P. Maruschak, et al., Appl. Sci. 13 (2023) 7247.
[22] R. Sangrody, M. Pouresmaeil, M. Marzband, et al., IEEE Trans. Power Electron. 35 (2020) 13068–13076.
[23] F. Dumur, Eur. Polym. J. 165 (2022) 110999.

[24] F. Dumur, Eur. Polym. J. 195 (2023) 112193.
[25] F. Dumur, Eur. Polym. J. 202 (2024) 112597.
[26] L. Deng, J. Qu, Prog. Org. Coat. 183 (2023) 107766.
[27] S. Gong, J. Hou, X. Wu, et al., Chem. Eng. J. 477 (2023) 146904.
[28] A.S. Hamidi, M.A. Hadis, W.M. Palin, Dent. Mater. 38 (2022) 1330–1343.
[29] K.T. Kitchin, J.L. Brown, Toxicol. 88 (1994) 31–49.
[30] R. Liu, S.A. Mabury, Environ. Sci. Technol. 52 (2018) 10089–10096.
[31] R. Liu, S.A. Mabury, Environ. Sci. Technol. Lett. 6 (2019) 702–707.
[32] M.C. Rhodes, J.R. Bucher, J.C. Peckham, et al., Food Chem. Toxicol. 45 (2007) 843–851.
[33] Q. Wu, K. Tang, Y. Xiong, et al., Macromol. Chem. Phys. 218 (2017) 1600484.
[34] Y. Wu, J. Ke, C. Dai, et al., Eur. Polym. J. 175 (2022) 111380.
[35] B. Zeng, Z. Cai, J. Lalevée, et al., Toxicol. in Vitro 72 (2021) 105103.
[36] H. Gu, W. Sun, J. Du, et al., Smart Mol. 2 (2024) e20230014.
[37] S.Y. Wang, Y.H. Pan, Y.C. Qu, et al., Smart Mol. 2 (2024) e20230024.
[38] M. Abdel-Halim, H. Tinsley, A.B. Keeton, et al., Bioorg. Chem. 104 (2020) 104322.
[39] H. Chen, G. Noirbent, Y. Zhang, et al., Polym. Chem. 11 (2020) 6512.
[40] L. Deng, J. Qu, Prog. Org. Coat. 174 (2023) 107240.
[41] T. Xue, H. Lu, H. Yuan, et al., Prog. Org. Coat. 162 (2022) 106587.
[42] S.C. Yen, Z.H. Lee, J.S. Ni, et al., Polym. Chem. 13 (2022) 3780.
[43] F. Dumur, Eur. Polym. J. 169 (2022) 111139.
[44] F. Dumur, Eur. Polym. J. 181 (2022) 111639.
[45] F. Dumur, Eur. Polym. J. 178 (2022) 111500.
[46] F. Dumur, Eur. Polym. J. 173 (2022) 111254.
[47] G. Noirbent, F. Dumur, Eur. Polym. J. 142 (2021) 110109.
[48] S. Gong, X. Wu, Q. Liao, et al., Green Chem. 25 (2023) 2730.
[49] X. Wu, S. Gong, Z. Chen, et al., Dyes Pigm. 205 (2022) 110556.
[50] T. Xue, Y. Li, L. Tang, et al., Dyes Pigm. 191 (2021) 109372.
[51] L. Hua, H. Qian, T. Lei, et al., Front. Bioeng. Biotechnol. 9 (2021) 796602.
[52] Y. Yang, X. Zhao, J. Yu, et al., Bioact. Mater. 6 (2021) 3962–3975.
[53] Z. Liu, S. Guo, L. Dong, et al., Mater. Today Bio 16 (2022) 100425.
[54] J.C. Dalton, N.J. Turro, Annu. Rev. Phys. Chem. 21 (1970) 499–560.
[55] M.A. El-Sayed, Acc. Chem. Res. 1 (2002) 8–16.
[56] A. Padwa, Acc. Chem. Res. 4 (2002) 48–57.
[57] A. Schonberg, A. Mustafa, Chem. Rev. 40 (2002) 181–200.
[58] H. Baumann, H.J. Timpe, V.E. Zubarev, et al., J. Photochem. 30 (1985) 487–500.